Journal of Molecular Graphics and Modelling 29 (2010) 137–147

Contents lists available at ScienceDirect

Journal of Molecular Graphics and Modelling

journal homepage: www.elsevier.com/locate/JMGM

Understanding the HIV-1 protease nelfinavir resistance mutation D30N in subtypes B and C through molecular dynamics simulations

Rosemberg O. Soares[a,b], Paulo R. Batista[b], Mauricio G.S. Costa[b], Laurent E. Dardenne[a], Pedro G. Pascutti[b], Marcelo A. Soares[c,d,*]

[a] Laboratório Nacional de Computação Científica, Petrópolis, Brazil
[b] Instituto de Biofísica Carlos Chagas Filho, Universidade Federal do Rio de Janeiro, Rio de Janeiro, Brazil
[c] Departamento de Genética, Universidade Federal do Rio de Janeiro, Rio de Janeiro, Brazil
[d] Programa de Genética, Instituto Nacional de Câncer, Rio de Janeiro, Brazil

ARTICLE INFO

Article history:
Received 25 August 2009
Received in revised form 12 May 2010
Accepted 14 May 2010
Available online 11 June 2010

Keywords:
HIV-1
Protease
Nelfinavir
Drug resistance
Subtype C
Molecular dynamics

ABSTRACT

A major concern in the antiretroviral (ARV) treatment of HIV infections with protease inhibitors (PI) is the emergence of resistance, which results from the selection of distinct mutations within the viral protease (PR) gene. Among patients who do not respond to treatment with the PI nelfinavir (NFV), the D30N mutation is often observed. However, several reports have shown that D30N emerges with different frequencies in distinct HIV-1 genetic forms or subtypes. In the present work, we analyzed the binding of NFV and the Gag substrate CA/p2 to PR from HIV-1 subtypes B and C through molecular dynamics (MD) simulations. The wild-type and drug-resistant D30N mutants were investigated in both subtypes. The compensatory mutations N83T and N88D, observed *in vitro* and *in vivo* when subtype C acquires D30N, were also studied. D30N appears to facilitate conformational changes in subtype B PR, but not in that from subtype C, and this could be associated with disestablishment of an α-helical region of the PR. Furthermore, the total contact areas of NFV or the CA/p2 substrate with the mutant PR correlated with changes in the resistance patterns and replicative capacity. Finally, we observed in our MD simulations that mutant PR proteins show different patterns for hydrophobic/van der Waals contact. These findings suggest that different molecular mechanisms contribute to resistance, and we propose that a single mutation has distinct impacts on different HIV-1 subtypes.

1. Introduction

Human immunodeficiency virus type 1 protease (HIV-1 PR) is a symmetric homodimeric aspartyl protease that cleaves the Gag and Gag-Pol viral polyproteins, allowing the virus to become infectious [1]. Drugs designed to inhibit HIV-1 PR have been developed in the past decades and their introduction into clinics to counter HIV infection has improved the treatment of HIV/AIDS patients [2]. The clinical success of these drugs is, however, frequently threatened by the occurrence of drug resistance mutations in the target enzyme. Currently, over 50 different drug resistance mutations at almost 30 different codon positions of HIV-1 PR have already been characterized [3], mainly due to the gene's highly polymorphic nature. Different HIV-1 subtypes possess distinct amino acid signatures and polymorphisms in the PR coding region [4–6], and the biological and phenotypic impact of these differences is yet to be fully appreciated [7].

The mutation D30N in HIV-1 PR is an amino acid change uniquely selected by virus exposure to the protease inhibitor (PI) nelfinavir (NFV) [8]. It confers reduced susceptibility of viruses to that drug *per se*, constituting a well established primary resistance mutation. Previous studies conducted in patients infected with distinct HIV-1 non-B subtypes have shown that these patients rarely develop the mutation compared with patients infected with subtype B [9–12]. The low frequency of D30N in subtype C has been associated with a more dramatic reduction in viral replicative capacity (RC) compared with subtype B counterparts carrying the same mutation [13]. Moreover, the occurrence of D30N in subtype C has been strongly associated with the compensatory mutations N88D and N83T *in vivo* and *in vitro*, respectively [12,13]. However, the structural hindrances governing the differences in replicative fitness and the requirement for those compensatory mutations are yet to be determined.

In the present work, the binding of NFV and of the Gag substrate cleavage site CA/p2 to both subtype B and C wild-type and D30N mutant PR was investigated by molecular dynamics (MD) and sub-

* Corresponding author at: Laboratório de Virologia Humana, CCS – Bloco A – sala A2-120, Cidade Universitária – Ilha do Fundão, 21949-570 Rio de Janeiro, RJ, Brazil. Tel.: +55 21 2562 6383; fax: +55 21 2562 6396.
E-mail address: masoares@biologia.ufrj.br (M.A. Soares).

1093-3263/$ – see front matter © 2010 Elsevier Inc. All rights reserved.
doi:10.1016/j.jmgm.2010.05.007

sequent structural *in silico* analyses. We also investigated subtype C PR structures harboring the compensatory mutations N83T or N88D. Our results point to structural differences in PR flap fluctuations, in hydrophilic and hydrophobic interactions at the active site and in secondary structure stabilities that help to elucidate the physical impact of D30N and of its accessory mutations in HIV-1 PR of distinct subtypes.

2. Methodology

2.1. Construction of PR models

The starting structures of the HIV-1 subtype B PR complexed with NFV and with the CA/p2 substrate were taken from atomic coordinate entries available in the Protein Data Bank (PDB) under accession codes 1OHR [14] and 1F7A [15], respectively. As experimentally determined structures for the PR mutants were not available, we used the comparative molecular modeling (CMM) for obtaining target structures. The crystal structure 1OHR was used as template (including the crystallographic water molecules and inhibitor coordinates) for constructing the ConsC (WT subtype C) by substituting the following PR amino acids using CCM, which differ between the consensus of subtypes B and C (I15V, M36I, R41K, H69K, L89 M and I93L), after the alignment with the template sequence [6]. In addition, the following mutant structures were modeled: subtype B with D30N (B-D30N), subtype C with D30N (C-D30N), subtype C with D30N and N83T (C-D30N/N83T), subtype C with D30N and N88D (C-D30N/N88D) and ConsC (WT). All structural models were built with the Swiss-Model and Swiss-PDB Viewer [16] using CMM. The structure 1F7A was used as template to construct the same PR described above, complexed with substrate. All models were validated by stereochemistry with the PROCHECK program [17] and energetically (see Suppl. Fig. 1) by calculating the DOPE score with Modeller v.9.7 [18] and the *z*-scores with the ProSa-Web server [19]. The *z*-score indicates overall model quality (Suppl. Fig. 1B). Its value is displayed in a plot that contains the *z*-scores of all experimentally determined protein chains in current PDB (Suppl. Fig. 1A). It can be used to check whether the *z*-score of each model is within the range of scores typically found for native proteins of similar size, including the scores calculated from the template structures.

2.2. Parameter generation for NFV

Since the topology of NFV was not publicly available for the GROMOS96 [20] force field, we initially used the PRODRG server [21] to generate a first set of parameters for bonds and angles based on the GROMOS87 force field [22]. Consequently, it was necessary to fit such parameters to GROMOS96 by means of previously determined parameters for groups similar to NFV. For the atom partial charge determination, we performed *ab initio* calculations using the GAUSSIAN94 program [23], applying the base B3LYP/6-31G** with option CHELPG, and assuming a null total charge for NFV.

To validate ligand parameters, we performed a preliminary MD simulation of NFV alone in both vacuum and within an explicit water box to check if torsions, angles and partial charges were consistent. The ligand structure did not change significantly in such conditions. The full topology is provided as Supplementary Material (Supplementary File 1).

2.3. Molecular dynamics simulations

Molecular mechanic potential energy minimizations and molecular dynamics (MD) simulations were performed with the program package GROMACS v. 3.3.1, using the GROMOS96 (43A1) force field, the SPC water model [24] and the leap-frog integration scheme. The solvation procedure was performed with a layer of at least 15 Å around the PR–ligand complex (approximately 11,350 water molecules), in a cubic box (≈380 nm^3), for periodic boundary conditions, totalizing approximately 36,000 atoms. An appropriate number (5–9, according to the protein total charge of each system) of chloride counter-ions were added to neutralize the system.

Before the MD simulations, an energy minimization procedure was split into three different steps. First, an energy minimization using the steepest-descent algorithm was made, allowing the solvent to relax while restraining the protein and ligand heavy atoms to their original positions with a harmonic potential. Then, another minimization using steepest-descent with no restraints was performed, allowing relaxation of the entire system. Finally, an energy minimization procedure with all restraints already removed was conducted, using the conjugate gradient method until reaching a gradient of 2.39 kcal mol^{-1} $Å^{-1}$.

After the minimization process, two stages of equilibration were conducted: a 500 ps MD with protein non-hydrogen atoms positions restrained to allow the formation of solvation layers and another of 2 ns without positional restriction. This second step is important for the system to accommodate the thermodynamic conditions imposed in the simulation. After those equilibration stages, an MD simulation of 8 ns was conducted for further analysis.

All MD simulations applied the constraint algorithms SETTLE [25] and LINCS [26]. The LINCS algorithm was used to constrain all the covalent bonds in non-water molecules, while the SETTLE algorithm was used to constrain bond lengths and angles in water molecules. The temperature was maintained at 300 K and pressure at 1 atm by using the Berendsen weak coupling approach [27]. For Coulomb interactions, the reaction field correction term [28] was employed, with a dielectric constant set to 54 [29]. Cutoff values of 1.2 Å and 1.4 Å were used for van der Waals and Coulomb interactions, respectively. According to previous kinetics and MD studies of HIV-1 PR [30–32], only the catalytic ASP124 was protonated.

All molecular structures were inspected using the programs VMD [33], MOLMOL [34] and PyMOL [35]. VMD was used for the visualization, manipulation and inspection of structures, for setting up the spatial orientation of the complexes and for aligning their principal axes to the Cartesian axes.

The secondary structures were calculated for each of the modeled structures complexed with NFV or substrate using the program Database of Secondary Structure in Proteins (DSSP) [36].

2.4. Intermolecular surface

In order to calculate the intermolecular contact surface areas from the MD trajectories of the complexes between PR and NFV or CA/p2 substrate, we used the program SURFINMD [37], based on Connolly's algorithm [38]. From the solvent accessible surface (SAS) of the protein and ligand, it is possible to determine the intermolecular surface as being the intersection between the SAS of the ligand and the SAS of the protein, i.e., the sum of the protein/ligand intersection areas, close enough to avoid the allocation of a water molecule. Contacts were classified as hydrophobic or hydrophilic depending on the nature of the PR and NFV or substrate atoms/residues involved in the contact.

2.5. MM/PBSA calculations

The binding free energy was calculated using the MM/PBSA approach [39], in which ΔG is obtained according to:

$$\Delta G_b = \Delta E_{MM} + \Delta G_{sol} - T\Delta S \quad (1)$$

Here, ΔG_b is the binding free energy in solution which is composed by the molecular mechanics interaction energy (ΔE_{MM}), the solvation free energy (ΔG_{sol}) and the conformational entropy contribution to binding ($-T\Delta S$). ΔG_{MM} corresponds to the sum of

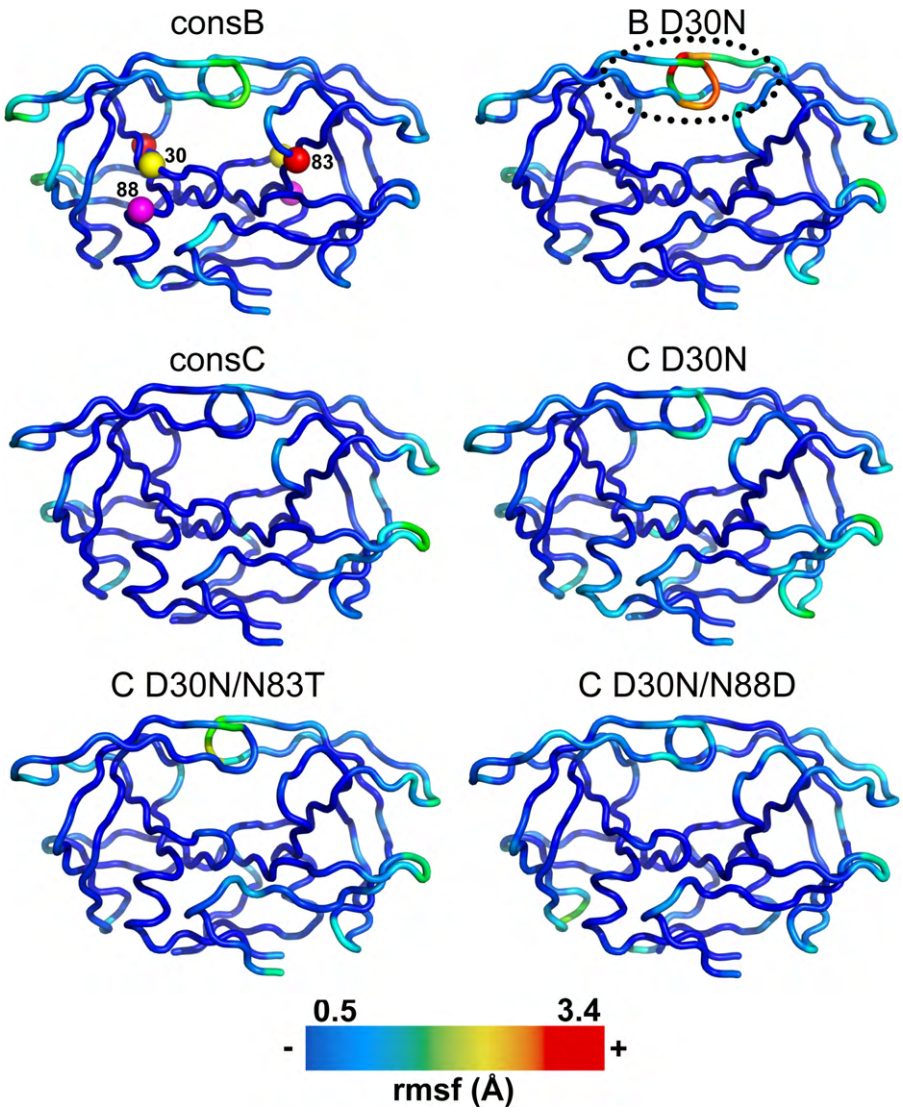

Fig. 1. Three-dimensional structural representation of the HIV-1 protease backbone fluctuations for each system, when complexed with NFV. The backbone RMSF is represented by tubes, and the color corresponds to the magnitude of the deviation accordingly to the scale bar. The NFV resistance-associated amino acid positions 30 (yellow), 83 (red) and 88 (magenta) studied herein are drawn in colored spheres at the upper left panel (ConsB). The enhanced fluctuating structure of the flaps in the B-D30N mutant (upper right panel) is circled.

electrostatic (ΔE_{elec}) and van der Waals (ΔE_{vdw}) interaction energies between protein and ligand as follows:

$$\Delta E_{MM} = \Delta E_{elec} + \Delta E_{vdw} \quad (2)$$

The solvation free energy contribution can be decomposed in two parts, the electrostatic ($\Delta G_{sol/elec}$) and the nonpolar ($\Delta G_{sol/np}$) terms:

$$\Delta G_{sol} = \Delta G_{sol/elec} + \Delta G_{sol/np} \quad (3)$$

The electrostatic term is obtained with the APBS software [40], which solves the Poisson–Boltzmann equation numerically and calculates the electrostatic energy according to the electrostatic potential. It was given a dieletric constant of 1 for the interior of the protein. The reference and the solvated systems had a solvent dieletric of 1 and 80, respectively. The electrostatic energy of the reference system was subtracted from that of the solvated system to yield the solvation energy. The nonpolar contribution of the solvation free energy is computed as a function of the solvent accessible area (SAS), as follows [41]:

$$\Delta G_{sol/np} = \gamma(SAS) + b \quad (4)$$

In this equation, $y = 0.00542$ kcal/mol Å^2 and $b = 0.92$ kcal/mol. The SAS was estimated using a 1.4 Å solvent probe radius with the *g_sas* module of GROMACS. The MM/PBSA calculations were performed in 100 snapshots collected from the last 200 ps of each trajectory.

3. Results

3.1. Conformational changes in PR complexes with NFV and substrate

To clarify the structural effects of mutations at residues 30, 83 and 88 of HIV-1 PR on its interaction with NFV and with a natural substrate, the root mean squared fluctuation (RMSF) values were calculated for each wild-type PR (consensus sequence for each subtype) and for the mutant structures. In PR–NFV complexes, a conformational change of the flaps (around residues 50 and 50′) was more pronounced in the B-D30N mutant compared with the remaining structures (Fig. 1). When the PR–substrate complex structures were compared, only slight conformational changes were found for all structures (Fig. 2), except for the B-D30N mutant,

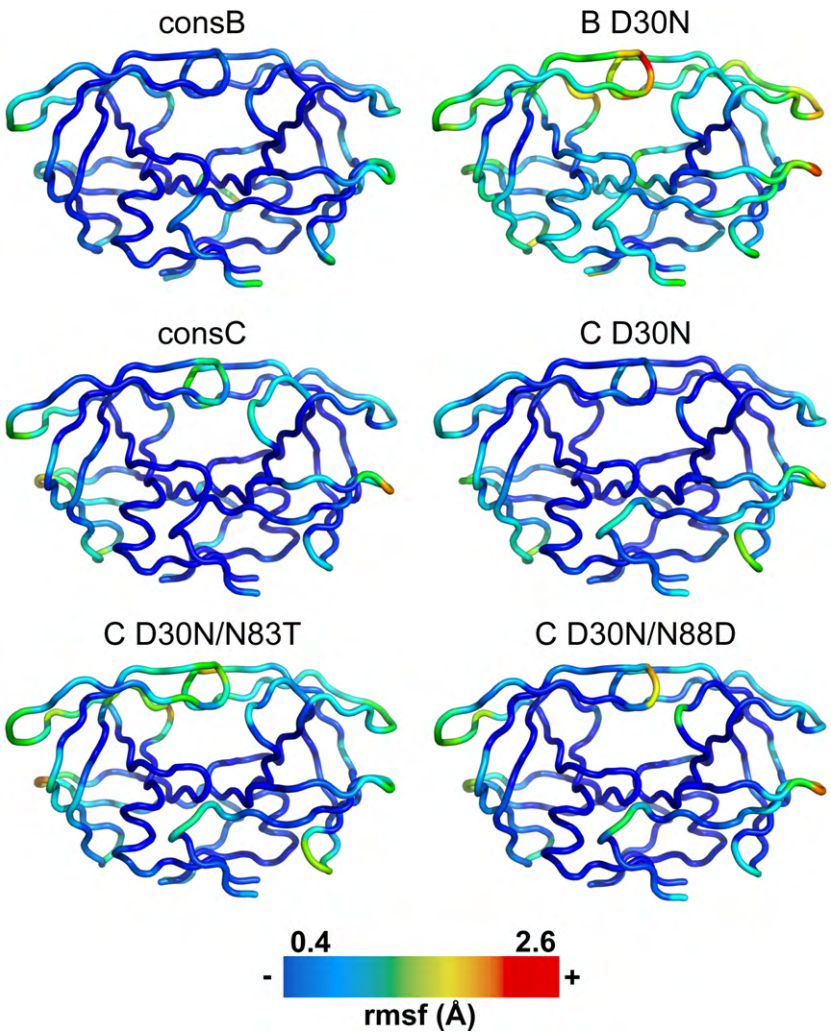

Fig. 2. Three-dimensional structural representation of the HIV-1 protease backbone fluctuations for each system, when complexed with the CA/p2 substrate. The RMSF fluctuations and coloring of the structures are represented as in Fig. 1.

where the overall flexibility was higher, mainly in the flaps (but not only in the tips as when bound to NFV – see also Fig. 1). These results suggest that binding to a natural PR substrate is not strongly impaired in any of the structures, but B-D30N has impaired stability when complexed with NFV.

We next analyzed whether the NFV-associated mutations caused changes in the secondary structure of HIV-1 PR in subtypes B and C. All the analyses were performed for a period of 8 ns (after 2 ns of unrestrained MD equilibration). However, the stability of the secondary structures was examined during the entire period (10 ns). PR was stabilized in all our simulated models prior to the dynamics tests (data not shown). Interestingly, among the PR–NFV complexes, the B-D30N mutant showed a strong disorganization of a α-helical stretch between residues 89′ and 94′, a phenomenon not seen in the remaining complexes (Fig. 3). When the dynamics of the PR–substrate structures were compared, only C-D30N showed a α-helical disorganization at an adjacent region, comprising residues 84′ to 90′ (Fig. 4).

3.2. Intermolecular contact surface areas between PR and ligands

We next evaluated the intermolecular contacts of the PR binding cavity with the ligands. Tables 1 and 2 depict the total, hydrophobic and hydrophilic contacts in each modeled structure with NFV and the CA/p2 substrate, respectively. The majority of the buried residues are hydrophobic when the structures of both subtypes are complexed with NFV. D30N alone strongly impairs the overall PR area of interaction with NFV in both B and C subtypes. In B-D30N, there was no dominance of the hydrophobic character of the residues involved in the interactions of the lost contacts. On the other hand, in the C-D30N mutant, the reduction in the contact with NFV was primarily of a hydrophobic nature (Table 1). Among the structures complexed with the CA/p2 substrate, the double mutant C-D30N/N83T was the most affected by the loss of hydrophobic contacts. The C-D30N/N88D double mutation hardly affected the buried residues complexed with NFV and with substrate when compared with C-D30N. In fact, a slight increase in the total contact area was observed with the substrate (Table 2).

3.3. Hydrogen bonds between NFV and PR

In PR–ligand interactions, hydrogen bonds play a crucial role in stabilizing the complex, both with the substrate and with NFV [14,15]. Therefore, we wanted next to study the hydrogen bond framework of our modeled structures, in particular the one involving the ligand and the catalytic aspartic acid residue 25 of PR. Both direct and water-mediated interactions were investigated. This analysis showed that mutation D30N affected these interactions in both B and C subtype mutants. The intensity of this effect, however, was different for each subtype (Table 3). Of note, the

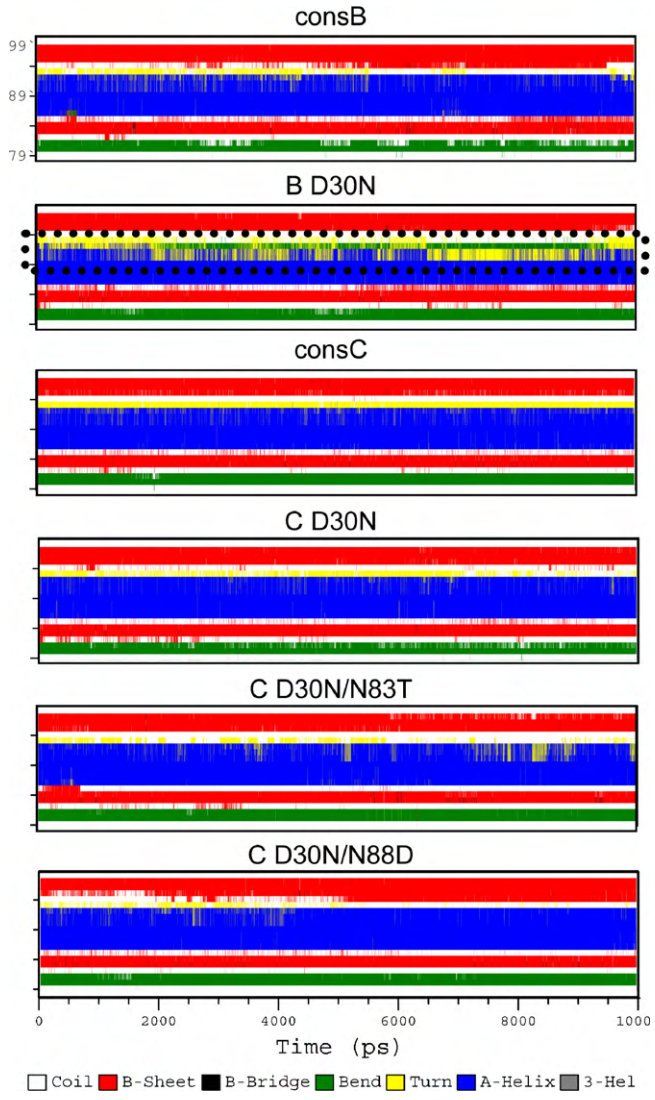

Fig. 3. HIV-1 PR C-terminal portion secondary structure patterns along the MD for each system complexed with NVF. White, green and yellow represent stretches in random conformations; residues in blue represent α-helices and those in red are β-sheet conformations. The *X*-axis represents the MD trajectory time (in ps), while the residue numbers are shown on the *Y*-axis. Only the protein region spanning amino acids 79′–99′ is shown. The boxed area in the B-D30N structure shows an α-helix region with the highest variation observed in the secondary structures.

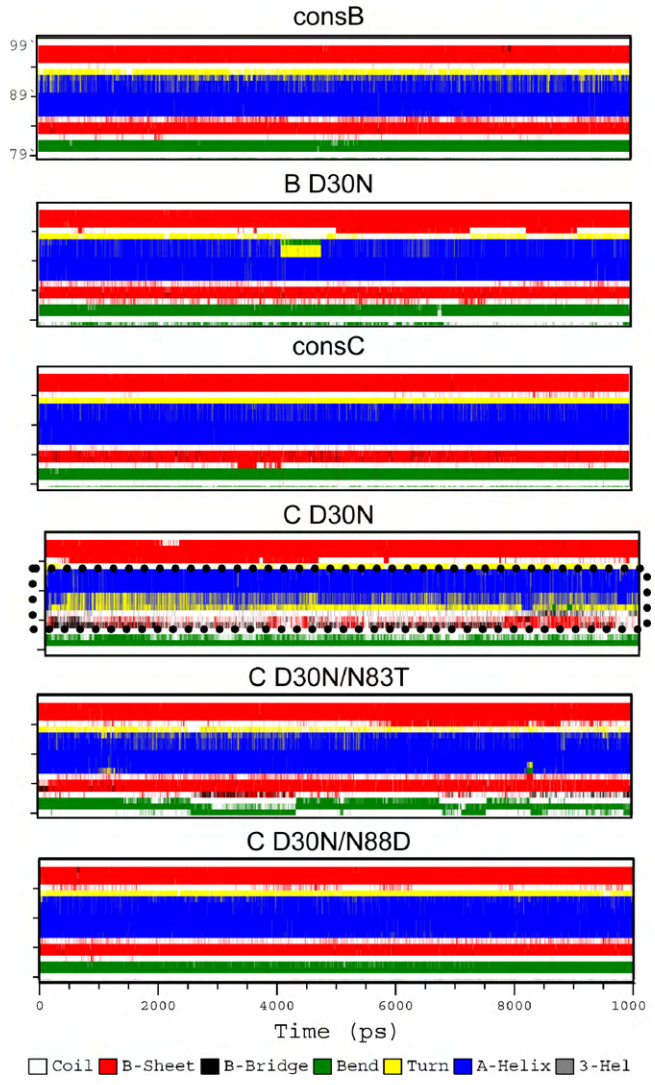

Fig. 4. HIV-1 PR C-terminal portion secondary structure patterns along the MD for each system complexed with the CA/p2 substrate. The color codes and the protein region shown are the same as in Fig. 3. The boxed area in the C-D30N structure shows an α-helix region with the highest variation observed in the secondary structures.

interaction between the N37 of the NFV P2 group with ASP25 of the enzyme was strong in the wt viruses (ConsB and ConsC), but absent in B-D30N and in C-D30N/N88D mutants. Moreover, hydrogen bonds between the NFV P2 group and residue 30 of the enzyme were strongly reduced in the mutants compared with their wild-type counterparts. The P1′ group of NFV interacted almost all the time with ASP25 in the wild-type B and C PR, and it was barely affected by the mutations in both subtypes. These observations were not paralleled in the systems complexed with the substrate CA/p2 (Table 4). In those cases, a rearrangement of the hydrogen bonds network between the substrate and the PR mutants occurred. Generally, the B-D30N mutant presented a decreased number and time-prevalence of hydrogen bonds, mainly in the residues of the flap tips, notably affecting the flexibility of this region that presented the higher fluctuations. However, the establishment of new contacts that remained stable during the simulation has also occurred, consisting of a rearrangement of contacts as in the other systems.

3.4. PR binding sites for NFV and substrate

Based on the contact surface analysis between PR and ligands, we have also calculated which residues were interacting specifi-

Table 1
Hydrophilic, hydrophobic and total interaction areas between subtype B and C PRs and NFV.

Interaction area (Å²)	ConsB	B-D30N	ConsC	C-D30N	C-D30N/N83T	C-D30N/N88D
Hydrophobic	367.4	284.9 (−82.5)[a]	377.8	295.7 (−82.1)	328.1 (−49.7)	381.2 (+3.4)
Hydrophilic	251.0	175.8 (−75.2)	252.0	219.6 (−32.4)	252.3 (+0.3)	264.2 (+12.2)
Total	618.4	460.7 (−157.7)	629.8	515.3 (−114.5)	580.4 (−49.4)	645.4 (+15.6)

[a] Numbers in parentheses denote differences between each mutant PR and its respective wild-type (ConsB or ConsC) counterpart.

Table 2
Hydrophilic, hydrophobic and total interaction areas between subtype B and C PRs and the CA/p2 substrate.

Interaction Area (Å^2)	ConsB	B-D30N	ConsC	C-D30N	C-D30N/N83T	C-D30N/N88D
Hydrophobic	546.0	527.7 (−18.3)[a]	580.0	599.0 (+19.0)	425.7 (−154.3)	614.7 (+34.7)
Hydrophilic	543.0	489.0 (−54.0)	373.5	397.8 (+24.3)	413.4 (+39.9)	415.2 (+41.7)
Total	1089.0	1016.7 (−72.3)	953.5	996.8 (+43.3)	839.1 (−114.4)	1029.9 (+76.4)

[a] Numbers in parentheses denote differences between each mutant PR and its respective wild-type (ConsB or ConsC) counterpart.

Table 3
Prevalence (%) of hydrogen bond interactions - direct (D) and water-mediated (WM) during the MD between PR and NFV.

NFV group	PR	ConsB		B-D30N		ConsC		C-D30N		C-D30N/N83T		C-D30N/N88D	
		D	WM	D	WM	D	WM	D	WM	D	WM	D	WM
P1′–O21	D25OD1/OD2	100	*	99.7	*	100	*	98.7	*	99.5	*	100	*
P1′–O21	A28N	*	*	*	*	*	*	*	*	27.6	*	*	*
P1′–O21	D124OD2	*	*	*	*	29.9	*	*	*	*	*	*	*
P2–N37	D25OD1/OD2	81.8	*	*	*	69.7	*	57.2	21.1	*	*	89.0	*
P2–O46	D29N	31.9	*	25.9	*	*	*	29.4	*	27.1	*	14.3	*
P2–O46	D29OD1/OD2	18.3	*	40.0	*	9.7	10.9	48.9	16.6	60.6	*	33.3	13
P2–O46	N/D30N	26.0	*	*	*	12.7	56.6	*	30.7	*	*	11.9	*
P2–O46	N30ND2	*	*	*	*	*	*	*	*	*	*	24.8	*
P2–O46	G48N	16.6	11.8	*	*	*	*	28.3	13.0	13.7	14.3	20.3	12.4
P2–O40	I50N	*	*	21.5	38.2	*	87.2	*	13.7	*	*	*	*
P2–O40	I149	*	*	*	*	*	*	*	*	*	41.3	*	*
P2–O40	G150N	*	*	*	*	*	*	*	*	26.6	52.3	*	*

Asterisks denote the lack of detectable bonds or bonds with prevalence below 10%.

cally with each chemical group of the ligand, thus determining the binding ligand subsite in each PR structure studied (Tables 5 and 6). Supplementary Figs. 2 and 3 show 2D schematic representations of these interactions in the context of a wild-type PR, respectively for NFV and the CA/p2 substrate. Interestingly, the B-D30N mutant lost interaction between relevant residues and NFV subsites. Namely, the interaction of the catalytic residue D25 and the NFV subsites S1, S1′ and S2′ are lost exclusively in B-D30N. All subtype C PR tested (wild-type and mutants) retained such interaction, providing further evidence of the resistant phenotype of B-D30N compared to the remaining protein systems. Other important sites related to PI drug resistance (such as PR residues V82 and I149 – the I50 of the second PR chain) also failed to interact with NFV S2 subsite. With respect to interactions with the CA/p2 substrate, the C-D30N mutant failed to show interaction between the catalytic residues D25 and D124 and both subsites S1 and S1′, whereas the double mutants C-D30N/N83T and C-D30N/N88D showed at least one of these catalytic residues interacting with the substrate.

3.5. Binding free energy calculations

The results shown above suggest that mutations in residues 30, 83 and 88 of PR are related to changes in the stability of the enzyme and also to alterations in the pattern of contacts established with the substrate or the inhibitor when compared to the wild-type enzyme.

Table 4
Prevalence (%) of hydrogen bond interactions – direct (D) and water-mediated (WM) – between PR and CA/p2 residues.

CA/p2 group	PR	ConsB		B-D30N		ConsC		C-D30N		C-D30N/N83T		C-D30N/N88D	
		D	WM	D	WM	D	WM	D	WM	D	WM	D	WM
P4–A200O	G48N	82.8	*	*	43	92.4	*	*	*	*	*	44.3	*
P4–A200N	D29OD1/OD2	*	*	79	*	*	*	*	*	*	*	*	*
P4–A200N	M46O	*	*	*	*	61.8	11.9	*	*	*	*	*	*
P3–R201O	D29N	*	26.6	*	*	*	*	80.8	*	*	*	12.5	*
P3–R201N	D29OD1/OD2	*	*	46.3	18.1	*	*	68.7	*	*	*	*	*
P3–R201NH1	G48O	32.2	*	*	*	*	*	*	*	*	*	*	*
P3−−R201NH1	G52O	42.3	*	*	*	*	*	*	*	*	*	*	*
P2–V202O	G49N	*	*	*	*	*	*	*	57.7	*	*	*	*
P2–V202O	I50N	*	*	63.4	*	*	*	*	68.3	79.8	*	*	*
P2–V202N	G48O	96.1	*	76.3	*	70.6	*	*	*	45.3	*	66.8	*
P1–LEU203O	I50N	*	*	*	*	*	*	*	*	*	*	82.3	11.9
P1–LEU203N	D25OD1/OD2	99.9	*	95.9	*	*	*	*	*	65.8	16.3	*	*
P1–LEU203O	I149N	*	*	*	*	*	*	92.1	*	92.3	*	*	*
P1′–ALA204N	D25OD1/OD2	*	*	97.9	*	*	*	*	*	71	14.3	*	22.4
P1′–ALA204O	I149N	*	68.4	*	*	15.9	17.6	*	*	*	*	*	*
P2′–G205OE1/2	D128N	46.3	*	97.4	*	93.3	*	100	*	99.6	*	95.8	*
P2′–G205OE1/2	D128OD2	*	*	96.9	*	*	*	*	*	*	*	*	*
P2′–G205OE1/2	D/N129N	75.8	*	93.2	*	*	50.7	96.6	*	98.8	*	97.3	*
P2′–G205OE1/2	D129OD2 or N129ND2	46.1	9.3	77.7	*	*	*	97.8	*	99	*	98.4	*
P2′–G205O	R186NH1/NH2	89.3	*	29.9	*	*	*	*	*	*	22	*	*
P2′–G205O	G126O	93.7	*	6.2	*	*	*	*	*	35	20.3	*	*
P3′–A206O	G147N	*	*	42	*	*	46.7	74.8	*	*	*	97	*
P3′–A206N	D147O	33	*	49	*	57.1	*	98.1	*	41.1	*	55.4	*
P4′–M207N	D128OD1/OD2	*	*	40.2	*	*	*	*	*	*	*	*	*

Table 5
Amino acid composition of each PR subsite when bound to NFV during MD*.

System	S2	S1	S1'	S2'
ConsB	I50, V82, A127, D128, D129, V131, I146, G147, G148, I149, I183	L23, D25, G27, A28, V32, I47, G48, I54, T80, P81, V82, I84, L122, D124, G126, A127, G148, I149, I183	D25, G27, A28, G48, I49, I50, R107, L122, D124, A127, V131, V181, I183	D25, G27, A28, A29, D30, V32, I47, G48, G49, I84, R87, D124, I149
BD30N	I50, A127, D128, D129, V131, I146, G147, G148, I183	G27, G48, I50, G52, L122, D124, G126, A127, G148, I149, V181, I183	I50, L122, D124, A127, V131, I146, G151, G153, P178, T179, P180, V181, I183	G27, A28, A29, D30, G48, G49, I50, R87, D124, V181
ConsC	I50, A127, D128, D129, V131, I146, G147, G148, I149, I183	L23, D25, G27, A28, V32, T80, P81, V82, I84, D124, G126, A127, G147, G148, I149, I183	D25, G27, A28, G48, I49, I50, L122, D124, A127, V131, T179, P180, V181, I183	D25, G27, A28, A29, D30, V32, I47, G48, G49, I50, I84, D124, I149, V181
CD30N	I50, G52, P81, V82, I146, G147, G148, I149	L23, D25, G27, A28, V32, I47, G48, G52, I54, T80, P81, V82, I84, D124, G126, G148, I149	D25, I49, I50, D124, A127, V131, I146, G147, G153, I183	D25, G27, A28, A29, D30, V32, I47, G48, G49, I50, I84, R87
CD30N/N83T	I50, D129, V131, I146, G147, G148, I149, G150, G151, I183	D25, G27, A28, V32, T80, P81, V82, I84, L122, D124, G147, G148, I149, I183	D25, G27, A28, G48, I49, I50, L122, D124, V131, I146, I149, G151, 153, T179, P180, V181, I183	D25, G27, A28, A29, D30, V32, I47, G48, G49, I50, I84, R87, I149, I150, V181
CD30N/N88D	I50, V82, A127, D128, D129, V131, I146, G147, G148, I149, I183	L23, D25, G27, A28, V32, I47, I54, T80, P81, V82, I84, D124, G126, A127, G148, I149, I183	D25, G27, A28, G48, I49, I50, L122, D124, A127, V131, I149, T179, P180, V181, I183	D25, G27, A28, A29, D30, V32, I47, G48, G49, I84, R87, D124, I149

* Amino acids constituting a subsite in the PR structure were considered when presenting an intermolecular surface area of at least 2.5 Å with each NFV group (P1, P2, etc.).

To estimate the effect of the loss of PR–ligand interactions in the D30N mutants on the binding free energy for substrate and NFV, MM/PBSA analyses were performed using 100 snapshots from the last 200 ps of each MD simulation. The calculated binding energies for NFV in Table 7 show that the D30N mutation weakens the interaction between protease and inhibitor for both studied HIV-1 subtypes.

From these analyses we obtained $\Delta\Delta G_b$ values of 9.6 and 8.3 kcal/mol for B-D30N and C-D30N mutants, respectively, in comparison to the consensus sequence for each subtype. The major loss of binding energy for the B mutant comes from van der Waals and electrostatic contributions, decreasing 16 and 4 kcal/mol, respectively. Nevertheless, these differences were considerably lower (~2 and 1.5 kcal/mol) for subtype C. The nonpolar solvation contribution was unfavorable in both mutants, while the polar solvation energy was more favorable in the B-D30N mutant in comparison to the wild-type (~11 kcal/mol).

With respect to the C-D30N/N88D double mutant, we observed that although the van der Waals contributions were more favorable in the mutant (~8 kcal), both electrostatic and polar solvation terms (ΔE_{elec} and $\Delta G_{sol/elec}$) were unfavorable (around −3.5 and −14 kcal/mol, respectively), which resulted in a decrease of ~10 kcal in the ΔG_b. The C-D30N/N83T mutant presented a similar profile to C-D30N/N88D, in which a loss of electrostatic contributions (~5 kcal) and unfavorable polar solvation (~2.5 kcal) are the main reasons that weakens the interaction of this mutant in comparison to the wild-type ($\Delta\Delta G_b$ = +7.1 kcal).

We also conducted binding energy evaluation in the PR-CA/p2 complexes (Table 8). We could note from this analysis that D30N led to more favorable interactions between PR and the CA/p2 substrate. This occurs due to a large gain in electrostatic interactions for both B and C subtypes (~+100 kcal/mol and ~+88 kcal/mol, respectively). Interestingly, for the double mutants, the electrostatic contributions were very close to the wild-type. Overall, our calculations revealed that all mutants presented stronger interactions if compared to their respective wild-type consensus sequences.

4. Discussion

An increasing body of evidence suggests that different HIV-1 subtypes may respond distinctly to interactions with antiretroviral drugs and may even follow distinct molecular pathways toward drug resistance [7]. One of the most striking differences observed thus far is the response of HIV-1 PR to NFV. It has been shown by several groups that D30N is selected at higher rates in subtype B than in other subtypes under NFV exposure. Non-B subtypes, including subtype C, rarely develop D30N [9–12], but do select for L90 M, a mutation conferring low-level cross-resistance to several PI [42]. Possible explanations for the low occurrence of D30N in subtype C are related to a more drastic impact on viral fitness [13]. We further investigated the structural determinants for this observation by comparing the molecular structures of wild-type and NFV-resistant mutants of HIV-1 PR in the context of B and C subtypes complexed with NFV and a natural ligand (the CA/p2 PR cleavage site) through MD.

Our simulations suggested that D30N affects primarily the flexibility of the PR flap region in subtype B complexed with NFV (Fig. 1). Such flexibility facilitates the loss of contact between the PR active site and the inhibitor, resulting in decreased affinity and destabilization of the ligand/PR interactions. This may explain at least in part the phenotypic resistance displayed by that mutant PR against NFV. This observation corroborates the idea that intense motions of flaps may confer resistance to NFV, by destabilizing the PR-inhibitor complex, as shown previously for other PI [43]. Of note, when B-D30N is complexed with the natural CA/p2 substrate, changes in the RMSF (Fig. 2) were smaller than those observed when bound to NFV (Fig. 1). This suggests that the mutant PR is able to interact more efficiently with the substrate, but not with the drug, an advantageous property for a resistant virus. For subtype C PR, we were unable to make any correlations with C-D30N function, as this mutant is only available *in silico*. Although C-D30N has a smaller loss of interaction with NFV than B-D30N compared with their WT counterparts, ConsC and ConsB, the analysis of C-D30N with the accessory mutations N83T or N88D provided more noteworthy data. N88D appears to reestablish more efficiently the interaction area with NFV than N83T, which is in agreement with a lower level of resistance provided by the former mutation compared with the latter, as seen by Gonzalez et al. [13]. The analysis of the total interaction area between the mutant PR and the natural CA/p2 substrate (Table 2) also provided insightful information correlating this interaction with the *in vitro* RC [13]. Of note, C-D30N carrying the accessory mutation N88D showed a higher interaction area with the substrate than the mutant carrying N83T. This was clearly correlated with the respective RC of those mutants described by Gonzalez et al. [13], being higher in the former.

Table 6
Amino acid composition of each PR subsite when bound to CA/p2 substrate during MD*.

System	S5	S4	S3	S2	S1	S1'	S2'	S3'	S4'
ConsB	D29, D30, K45, M46, I47, G48, F53, L76, P180	K45, M46, I47, G49, F53, I149	G27, A28, D29, D30, G48, G49, I50, G52, F53, P180, V181	D25, G27, A28, D29, D30, V32, I47, G48, G49, I50, V82, I84, I149	D25, G27, A28, D29, G49, I50, I84, L122, D124, G126, A127, V131, T179, P180, V181, I183	D25, G49, I50, P81, V82, N83, I84, D124, G126, A127, G147, G148, I149	K7, R8, L23, D25, I50, V82, G126, A127, D128, D129, G147, I149, R186	K7, R8, L23, P81, V82, G126, A127, D128, I149, R186	K7, R8, P81, V82, G147, F152
BD30N	D29, D30, K45, M46, I47, G48, Q58, T74, L76	A28, D29, D30, V32, K45, M46, I47, G49, F53, L76	D25, G27, A28, D29, D30, G48, G49, I50, R107, P180	D25, A28, V32, I47, G48, G49, I50, G54, V82, I84, I149	D25, G27, A28, G49, I50, I84, R107, D124, G126, A127, G147, I149	L23, D25, I50, P81, V82, I84, G126, A127, G147, I149	R8, L23, I50, V82, G126, A127, D128, D129, I146, G147, I149, R186	L23, I50, P81, V82, A127, D128, M145, I146, G147, G148, I149, F152, R186	R8, D128, D129, K144, M145, I146, G147, F152
ConsC	M46, I47, G48, F53	K45, M46, I47, G49, F53, L76, I149	D29, D30, G48, G49, F53, P178, P180	A28, D29, D30, V32, I47, G48, G49, I50, I149, V181	D25, G27, A28, D29, G48, G49, I50, I84, L122, D124, V131, I149, T179, P180, I183	L23, D25, A28, G49, I50, V82, I84, I146, G147, G148, I149	R8, L23, D25, I50, V82, G126, A127, D128, D129, V131, I146, G147, G148, R186	R8, L23, I50, P81, V82, D129, M145, G147, G148, I149, F152	R8, P81, V82, D128, K144, M145, G147, F152
CD30N	D29, G48, G49, G51, F53, P180, V181	D30, I47, G49, I50, F53, I149, P180, V181	D25, G27, A28, D29, D30, G49, I50, P180, V181, N182	A28, D29, D30, V32, I47, G48, G49, I50, G54, I84, I149, P180, V181	V32, G48, G49, I50, I54, P81, A127, V131, G147, G148, I149, V181, I183	I50, T80, P81, V82, I84, G147, G148, I149	R8, L23, P81, V82, A127, D128, D129, G147, G148, I149, R186	I50, P81, M145, I146, G147, G148, F152	D129, K144, I146, G147, F152
CD30N/N83T	G27, D29, R87, R107	G27, A28, D29, R87	D25, G27, A28, D29, G48, G49, I50, R107	D25, G27, A28, D29, V32, I47, G48, G49, I50, G54, I84, I149	D25, A28, G49, I50, I54, P81, I84, D124, G126, A127, G147, G148, I149	L23, D25, I50, I54, T80, P81, V82, I84, G126, G147, G148, I149	R8, L23, D25, P81, V82, G126, A127, D128, D129, G147, G148, I149, R186	R8, P81, V82, I146, G147, G148, I149, F152	K7, R8, D129, K144, M145, I146, G147, F152
CD30N/N88D	D29, D30, I47, L76, R87, P180, V181	D29, D30, M46, I47, G49, F53, L76, R87, V181	G27, A28, D29, D30, G48, G49, I50, F53, P180, V181	A28, D29, D30, V32, I47, G48, G49, I50, G54, I84, I149, P180, V181	G27, A28, G48, G49, I50, I54, P81, I84, D124, V131, G147, I149, T179, P180, V181, I183	D25, A28, G49, I50, I54, T80, P81, V82, I84, I146, G147, G148, I149	R8, L23, I50, P81, V82, A127, D128, D129, I146, G147, I149, R186	R8, I50, P81, V82, D128, D129, M145, I146, G147, G148, I149, F152	R8, D129, K144, M145, I146, G147, F152

* Amino acids constituting a subsite in the PR structure were considered when presenting an intermolecular surface area of at least 2.5 Å with each CA/p2 group (P1, P2, etc.).

Table 7
Binding energies (kcal/mol) between PR and NFV calculated with MM/PBSA.

Subtype	ΔE_{elec}	ΔE_{vdw}	$\Delta G_{sol/elec}$	$\Delta G_{sol/np}$	ΔG_b[a]	$\Delta\Delta G_b$[b]
ConsB	−33.7	−61.9	64.6	−5.4	−36.4	–
B-D30N	−29.6	−46.2	53.4	−4.3	−26.7	−9.7
ConsC	−37.1	−62.9	69.9	−5.7	−35.8	–
C-D30N	−35.3	−60.7	73.5	−5.1	−27.5	−8.3
C-D30N/N83T	−31.8	−63.8	72.4	−5.6	−28.7	−7.1
C-D30N/N88D	−33.2	−70.6	83.5	−5.8	−26.2	−9.6

[a] The entropic contribution, "$-T\Delta S$", is not included (see text for details).
[b] Difference from the consensus sequence of each subtype ($\Delta\Delta G_b = \Delta G_b^{(WT)} - \Delta G_b^{(mutant)}$).

Table 8
Binding energies (kcal/mol) between PR and CA/p2 calculated with MM/PBSA.

Subtype	ΔE_{elec}	ΔE_{vdw}	$\Delta G_{sol/elec}$	$\Delta G_{sol/np}$	ΔG_b[a]	$\Delta\Delta G_b$[b]
ConsB	−130.9	−61.9	192.1	−5.6	−6.3	–
B-D30N	−231.4	−70.6	181.1	−7.9	−128.7	122.5
ConsC	−114.4	−81.7	186.7	−7.2	−16.7	–
C-D30N	−202.1	−76.5	187.6	−7.0	−97.9	81.3
C-D30N/N83T	−153.5	−69.1	151.8	−6.4	−77.3	60.6
C-D30N/N88D	−140.8	−77.5	196.5	−7.3	−29.1	12.4

[a] $T\Delta S$ term not included.
[b] Difference from the consensus sequence of each subtype ($\Delta\Delta G_b = \Delta G_b^{(WT)} - \Delta G_b^{(mutant)}$.

In order to verify whether the PR mutants retained a stable structure when complexed to NFV and a natural substrate, we verified the maintenance of secondary structures throughout our simulations. Overall, stable secondary structures were observed. Interestingly, the B-D30N mutant displayed a significant disorganization in one of its α-helices (corresponding to residues 88′–92′) when complexed with NFV (Fig. 3). Conversely, disorganization in the same α-helix region was observed for C-D30N, but when complexed to CA/p2. Such variations are likely to influence the interaction between PR and its ligand or inhibitor. In the first case, this influence may promote resistance, while in the second it may cause an impaired accommodation of the substrate. Further studies are needed to elucidate the exact impact of α-helix destabilization on HIV-1 PR activity.

Our MD studies indicated that the drug resistance mutations under evaluation affect the conformation of the PR binding cavity and both hydrophilic and hydrophobic interactions at the enzyme's active site pocket. We have shown that changes in the NFV–PR complex decrease both types of contacts between NFV and the proteases B-D30N and C-D30N (Table 1). Interestingly, however, the reduction in the hydrophilic contacts of B-D30N with the drug was twice as high as for C-D30N. On the other hand, the double mutation D30N/N83T in subtype C caused losses of exclusively hydrophobic contacts (Tables 1 and 2) when complexed with either NFV or the CA/p2 substrate. In remarkable contrast, increases in both hydrophobic and hydrophilic contacts were seen in C-D30N/N88D. These results lead us to hypothesize that the secondary mutation N88D restores areas of molecular interaction initially lost due to the acquisition of D30N. This hypothesis corroborates the RC results that suggest that N83T and N88D are compensatory mutations [13].

It has been previously shown that the impairment of hydrogen bond formation between PR residue 30D and the m-phenol group of NFV causes a decrease in PR affinity to that drug [14]. In our simulations, we noticed that one hydrogen bond between the 25D and the nitrogen N37 of the P2 group was lost in the B-D30N mutant when compared with its respective wild-type PR (Table 3). Our data agree with the results obtained by Coman et al [44]. In that study, the authors found that both B and C D30N mutants had drastically increased K_i values compared to their wild-type counterparts, evidencing strong loss of affinity to NFV.

We analyzed the impact of NFV and substrate interaction with PR on the protein secondary structure dynamics. Notably, B-D30N-NFV and C-D30N-substrate complexes have undergone profound changes in a specific α-helix region that interacts with the ligands. These effects are in agreement with the reported behaviors of these mutants with respect to resistance and RC. B-D30N has an unstable interaction with NFV (a resistance phenotype), while C-D30N has an unstable interaction with the substrate (impaired RC).

We performed MD simulations for the wild-type B, B-D30N, wild-type C, C-D30N, C-D30N/N83T and C-D30N/N88D PR mutants to clarify the resistance phenotype of each mutant to NFV and their interaction with the CA/p2 substrate. Our data suggest that D30N confers NFV resistance by reducing hydrogen bond interactions between PR residue 30N and the P2 group of the drug, an event more pronounced in subtype B than in C. Changes in the interactions of the mutants with NFV were congruent with phenotypic resistance data, while changes in the PR-substrate intermolecular interactions (Table 4) corroborate viral RC data [13]. In other words, subtype B viruses carrying D30N in PR presented a lower number and time-prevalence of hydrogen bond interactions with the CA/p2 substrate.

The calculation of the relative binding affinities of the wild-type PR and the mutants in complex with NFV provided relevant information to understand the impact of the mutations on resistance to PI. Our calculations revealed that the D30N mutation results in weak interactions between PR and NFV in comparison to the wild-type. A possible explanation for the differences in the energetic contributions is that the loss of contacts between PR and the inhibitor resulted in a decrease of the van der Waals and electrostatic contributions (Table 7). This is also related to the decrease of nonpolar contributions in the mutants, which is related to the significant loss of hydrophobic contacts in these systems (Table 1). These data are in good agreement with experiments showing that mutations in this position confer resistance to NFV in subtype B [13]. In addition, it was possible to predict the affinities of the C-D30N mutant, which were comparable to those observed for the B-D30N mutant, suggesting a likely resistant phenotype for this mutant (Table 7).

The calculations on the C-D30N/N83T mutant revealed that these mutations resulted in a loss of approximately 7 kcal/mol of binding energy in comparison with the wild-type. This result may be explained by the loss of a hydrogen bond between D25 and NFV (Table 3). In addition, the reduced number of contacts established by the residue 30 may also explain the weak affinity of this mutant by the inhibitor (Table 5). Concerning the C-D30N/N88D, the weak binding energies are related to less favorable contributions of electrostatic origin ($\Delta G_{sol/elec}$) when compared with the wild-type (Table 7).

Our calculations for the PR-CA/p2 complexes (Table 8) showed that the D30N mutation favors the interactions between the enzyme and the substrate, by providing stronger electrostatic interactions than those observed for the wild-type sequences. However, the results obtained presented high fluctuations which led to difficulties in interpretation of data. This fact is most likely derived from (i) the increased flexibility of PR in the substrate bound simulations, predominantly in the flap region (mainly for the D30N mutants); see Fig. 2; and (ii) due to the larger size of the substrate compared to the inhibitor. Therefore, the loss of conformational entropy upon ligand binding is expected to be larger in the substrate bound PR than in the inhibitor complexes. Thus, the contributions of conformational entropy will likely present a major impact in binding of the PR/substrate complexes.

For both protease and inhibitor MM/PBSA analyses, the compensatory mutations failed to revert (even partially) the D30N affinity loss effect in binding. This could be in part due to entropic effects that were neglected in our calculations.

When the molecular surface interactions between the studied PRs and NFV or CA/p2 substrate were analyzed, interesting observations were made that could provide explanations to the phenotypic behavior of the individual proteins. For example, the loss of interaction between B-D30N D25 residue and NFV groups P1, P1′ and P2′ was indicative of an enhanced resistant phenotype displayed by this mutant compared to the other PRs (Table 5). Additional losses of interaction between B-D30N residues V82 and I149 (the latter being a residue in the flap region) were also observed.

When interactions with CA/p2 substrate were analyzed (Table 6), the C-D30N was the only mutant PR lacking interaction of the catalytic residues D25 and D124 with the substrate groups P1 and P1′, strongly providing evidence for the non-viability of this mutant *in vivo*. In addition, the destabilization of the C-D30N secondary structure (Fig. 4) further corroborates hindrance forces that may explain the distinct emergence rates of D30N in the PR of HIV-1 subtypes B and C.

5. Conclusions

This study has provided new insights into the molecular hindrances responsible for the low acquisition of PI-associated drug resistance mutation D30N in subtype C. Even with the co-occurrence of accessory mutations, subtype C PR is less prone than that of subtype B to accommodate the conformational changes required for D30N. This results in destabilization of secondary structures, along with the reduction of intermolecular contact areas between PR and NFV or a natural substrate. These changes may explain the more dramatic effects on the replicative fitness observed in previous *in vitro* studies. Our data thus provide insightful explanations for the differences observed in the impact of D30N in distinct HIV-1 subtypes.

Acknowledgements

The authors acknowledge the Brazilian agencies CNPq (Ministry of Science and Technology), CAPES (Ministry of Education) and FAPERJ (Rio de Janeiro State Science Foundation) for financial support. R.O.S., L.E.D. and M.A.S. also thank the Laboratório Nacional de Computação Científica (LNCC-MCT) for computational facilities and financial support. The sponsors of this study played no role in its design, in the collection, analysis and interpretation of data, in the writing of the report and in the decision to submit the paper for publication.

Appendix A. Supplementary data

Supplementary data associated with this article can be found, in the online version, at doi:10.1016/j.jmgm.2010.05.007.

References

[1] A. Wlodawer, J. Vondrasek, Inhibitors of HIV-1 protease: a major success of structure-assisted drug design, Annu. Rev. Biophys. Biomol. Struct. 27 (1998) 249–284.
[2] P.M. Colman, New antivirals drug resistance, Annu. Rev. Biochem. 78 (2009) 95–118.
[3] R.W. Shafer, J.M. Schapiro, HIV-1 drug resistance mutations: an updated framework for the second decade of HAART, AIDS Rev. 10 (2) (2008) 67–84.
[4] A. Holguin, E. Paxinos, K. Hertogs, C. Womac, V. Soriano, Impact of frequent natural polymorphisms at the protease gene on the in vitro susceptibility to protease inhibitors in HIV-1 non-B subtypes, J. Clin. Virol. 31 (3) (2004) 215–220.
[5] R. Kantor, D.A. Katzenstein, B. Efron, A.P. Carvalho, B. Wynhoven, P. Cane, J. Clarke, S. Sirivichayakul, M.A. Soares, J. Snoeck, C. Pillay, H. Rudich, R. Rodrigues, A. Holguin, K. Ariyoshi, M.B. Bouzas, P. Cahn, W. Sugiura, V. Soriano, L.F. Brigido, Z. Grossman, L. Morris, A.M. Vandamme, A. Tanuri, P. Phanuphak, J.N. Weber, D. Pillay, P.R. Harrigan, R. Camacho, J.M. Schapiro, R.W. Shafer, Impact of HIV-1 subtype and antiretroviral therapy on protease and reverse transcriptase genotype: results of a global collaboration, PLoS Med. 2 (4) (2005) e112.
[6] M.A. Soares, T. De Oliveira, R.M. Brindeiro, R.S. Diaz, E.C. Sabino, L. Brigido, I.L. Pires, M.G. Morgado, M.C. Dantas, D. Barreira, P.R. Teixeira, S. Cassol, A. Tanuri, A specific subtype C of human immunodeficiency virus type 1 circulates in Brazil, Aids 17 (1) (2003) 11–21.
[7] M.A. Soares, Drug resistance differences among HIV types and subtypes: a growing problem, Future HIV Therapy 2 (6) (2008) 579–593.
[8] A.K. Patick, M. Duran, Y. Cao, D. Shugarts, M.R. Keller, E. Mazabel, M. Knowles, S. Chapman, D.R. Kuritzkes, M. Markowitz, Genotypic and phenotypic characterization of human immunodeficiency virus type 1 variants isolated from patients treated with the protease inhibitor nelfinavir, Antimicrob. Agents Chemother. 42 (10) (1998) 2637–2644.
[9] P.A. Cane, A. de Ruiter, P. Rice, M. Wiselka, R. Fox, D. Pillay, Resistance-associated mutations in the human immunodeficiency virus type 1 subtype c protease gene from treated and untreated patients in the United Kingdom, J. Clin. Microbiol. 39 (7) (2001) 2652–2654.
[10] Z. Grossman, E.E. Paxinos, D. Averbuch, S. Maayan, N.T. Parkin, D. Engelhard, M. Lorber, V. Istomin, Y. Shaked, E. Mendelson, D. Ram, C.J. Petropoulos, J.M. Schapiro, Mutation D30N is not preferentially selected by human immunodeficiency virus type 1 subtype C in the development of resistance to nelfinavir, Antimicrob. Agents Chemother. 48 (6) (2004) 2159–2165.
[11] W. Sugiura, Z. Matsuda, Y. Yokomaku, K. Hertogs, B. Larder, T. Oishi, A. Okano, T. Shiino, M. Tatsumi, M. Matsuda, H. Abumi, N. Takata, S. Shirahata, K. Yamada, H. Yoshikura, Y. Nagai, Interference between D30N and L90M in selection and development of protease inhibitor-resistant human immunodeficiency virus type 1, Antimicrob. Agents Chemother. 46 (3) (2002) 708–715.
[12] C. Sukasem, V. Churdboonchart, W. Sukeepaisarncharoen, W. Piroj, T. Inwisai, M. Tiensuwan, W. Chantratita, Genotypic resistance profiles in antiretroviral-naive HIV-1 infections before and after initiation of first-line HAART: impact of polymorphism on resistance to therapy, Int. J. Antimicrob. Agents 31 (3) (2008) 277–281.
[13] L.M. Gonzalez, R.M. Brindeiro, R.S. Aguiar, H.S. Pereira, C.M. Abreu, M.A. Soares, A. Tanuri, Impact of nelfinavir resistance mutations on in vitro phenotype, fitness, and replication capacity of human immunodeficiency virus type 1 with subtype B and C proteases, Antimicrob. Agents Chemother. 48 (9) (2004) 3552–3555.
[14] S.W. Kaldor, V.J. Kalish, J.F. Davies, 2nd, B.V. Shetty, J.E. Fritz, K. Appelt, J.A. Burgess, K.M. Campanale, N.Y. Chirgadze, D.K. Clawson, B.A. Dressman, S.D. Hatch, D.A. Khalil, M.B. Kosa, P.P. Lubbehusen, M.A. Muesing, A.K. Patick, S.H. Reich, K.S. Su, J.H. Tatlock, Viracept (nelfinavir mesylate, AG1343): a potent, orally bioavailable inhibitor of HIV-1 protease, J. Med. Chem. 40 (24) (1997) 3979–3985.
[15] M. Prabu-Jeyabalan, E. Nalivaika, C.A. Schiffer, How does a symmetric dimer recognize an asymmetric substrate? A substrate complex of HIV-1 protease, J. Mol. Biol. 301 (5) (2000) 1207–1220.
[16] N. Guex, M.C. Peitsch, SWISS-MODEL and the Swiss-PdbViewer: an environment for comparative protein modeling, Electrophoresis 18 (15) (1997) 2714–2723.
[17] R.A. Laskowski, J.A. Rullmannn, M.W. MacArthur, R. Kaptein, J.M. Thornton, AQUA and PROCHECK-NMR: programs for checking the quality of protein structures solved by NMR, J. Biomol. NMR 8 (4) (1996) 477–486.
[18] N. Eswar, B. Webb, M.A. Marti-Renom, M.S. Madhusudhan, D. Eramian, M.Y. Shen, U. Pieper, A. Sali, Comparative protein structure modeling using MODELLER, Curr. Protoc. Protein Sci. (2007) (Chapter 2, Unit 2 9).
[19] M. Wiederstein, M.J. Sippl, ProSA-web: interactive web service for the recognition of errors in three-dimensional structures of proteins, Nucleic Acids Res. 35 (2007) W407–W410, Web Server issue.
[20] W.F. Van Gunsterem, S.R. Billeter, A.A. Eising, P.H. Hünenberger, P. Krüger, A.E. Mark, A.E.X. Scott, I.G. Tironi, Biomolecular Simulation: The GROMOS96 manual and User Guide, Vdf Hochschulverlag AG, Zürich, 1996.
[21] D.M. van Aalten, R. Bywater, J.B. Findlay, M. Hendlich, R.W. Hooft, G. Vriend, PRODRG, a program for generating molecular topologies and unique molecular descriptors from coordinates of small molecules, J. Comput. Aided Mol. Des. 10 (3) (1996) 255–262.
[22] W.F. Van Gunsterem, H.J.C. Berendsen, Groningen Molecular Simulation (GROMOS) Library Manual, BIOMOS, Groningen, 1987.
[23] M.J. Frisch, G.W.H. Trucks, B. Schlegel, GAUSSIAN94, Revision B. 1, Gaussian, Inc., Pittsburg, 1995.
[24] H.J.C. Berendsen, J.P.M. Postma, W.F.V. Gunsteren, J. Hermans, Interaction models for water in relation to protein hydration, in: B. Pullman (Ed.), Intermolecular Forces, vol. 1, Reidel, Dordrecht, 1981, pp. 331–342.
[25] S. Miyamoto, P.A. Kollman, Settle: an analytical version of the SHAKE and RATTLE algorithm for rigid water models, Journal of Computational Chemistry 13 (8) (1992) 952–962.
[26] B. Hess, H. Bekker, H.J.C. Berendsen, J.G.E.M. Fraaije, LINCS: a linear constraint solver for molecular simulations, J. Comput. Chem. 18 (12) (1997) 1463–1472.
[27] H.J.C. Berendsen, J.P.M. Postma, W.F. Van Gunsteren, A. Dinola, J.R. Haak, Molecular–dynamics with coupling to an external bath, J. Chem. Phys. 81 (1984) 3684–3690.
[28] H. Schreiber, O. Steinhauser, Taming cut-off induced artifacts in molecular dynamics studies of solvated polypeptides. the reaction field method, J. Mol. Biol. 228 (3) (1992) 909–923.
[29] P.E. Smith, W.F. van Gunsteren, Consistent dielectric properties of the simple point charge and extended simple point charge water models at 277 and 300k, J. Chem. Phys. 100 (4) (1994) 3169–3174.

[30] P.R. Batista, A. Wilter, E.H. Durham, P.G. Pascutti, Molecular dynamics simulations applied to the study of subtypes of HIV-1 protease common to Brazil, Africa, and Asia, Cell Biochem. Biophys. 44 (3) (2006) 395–404.
[31] L.J. Hyland, T.A. Tomaszek Jr., T.D. Meek, Human immunodeficiency virus-1 protease. 2. Use of pH rate studies and solvent kinetic isotope effects to elucidate details of chemical mechanism, Biochemistry 30 (34) (1991) 8454–8463.
[32] L.J. Hyland, T.A. Tomaszek Jr., G.D. Roberts, S.A. Carr, V.W. Magaard, H.L. Bryan, S.A. Fakhoury, M.L. Moore, M.D. Minnich, J.S. Culp, et al., Human immunodeficiency virus-1 protease. 1. Initial velocity studies and kinetic characterization of reaction intermediates by 18O isotope exchange, Biochemistry 30 (34) (1991) 8441–8453.
[33] W. Humphrey, A. Dalke, K. Schulten, VMD: visual molecular dynamics, J. Mol. Graph. 14 (1) (1996) 33–38, 27-8.
[34] R. Koradi, M. Billeter, K. Wuthrich, MOLMOL: a program for display and analysis of macromolecular structures, J. Mol. Graph. 14 (1) (1996) 51–55, 29–32.
[35] W.L. DeLano, S. Bromberg, PyMOL User's Guide, DeLano Scientific LLC, San Francisco, 2004.
[36] W. Kabsch, C. Sander, Dictionary of protein secondary structure: pattern recognition of hydrogen-bonded and geometrical features, Biopolymers 22 (12) (1983) 2577–2637.
[37] P.A. Valiente, P.R. Batista, A. Pupo, T. Pons, A. Valencia, P.G. Pascutti, Predicting functional residues in *Plasmodium falciparum* plasmepsins by combining sequence and structural analysis with molecular dynamics simulations, Proteins 73 (2) (2008) 440–457.
[38] M.L. Connolly, Solvent-accessible surfaces of proteins and nucleic acids, Science 221 (4612) (1983) 709–713.
[39] P.A. Kollman, I. Massova, C. Reyes, B. Kuhn, S. Huo, L. Chong, M. Lee, T. Lee, Y. Duan, W. Wang, O. Donini, P. Cieplak, J. Srinivasan, D.A. Case, T.E. Cheatham 3rd, Calculating structures and free energies of complex molecules: combining molecular mechanics and continuum models, Acc. Chem. Res. 33 (12) (2000) 889–897.
[40] N.A. Baker, D. Sept, S. Joseph, M.J. Holst, J.A. McCammon, Electrostatics of nanosystems: application to microtubules and the ribosome, Proc. Natl. Acad. Sci. USA 98 (18) (2001) 10037–10041.
[41] M.F. Sanner, A.J. Olson, J.C. Spehner, Reduced surface: an efficient way to compute molecular surfaces, Biopolymers 38 (3) (1996) 305–320.
[42] V.A. Johnson, F. Brun-Vezinet, B. Clotet, H.F. Gunthard, D.R. Kuritzkes, D. Pillay, J.M. Schapiro, D.D. Richman, Update of the drug resistance mutations in HIV-1, Top. HIV Med. 16 (5) (2008) 138–145.
[43] F. Liu, A.Y. Kovalevsky, Y. Tie, A.K. Ghosh, R.W. Harrison, I.T. Weber, Effect of flap mutations on structure of HIV-1 protease and inhibition by saquinavir and darunavir, J. Mol. Biol. 381 (1) (2008) 102–115.
[44] R.M. Coman, A.H. Robbins, M.A. Fernandez, C.T. Gilliland, A.A. Sochet, M.M. Goodenow, R. McKenna, B.M. Dunn, The contribution of naturally occurring polymorphisms in altering the biochemical and structural characteristics of HIV-1 subtype C protease, Biochemistry 47 (2) (2008) 731–743.